ELSEVIER

Journal of Nuclear Materials 264 (1999) 180–197

journal of nuclear materials

Deuterium trapping in deep traps of differently oriented pyrolytic graphite exposed to D_2 gas at 1473 K

V.N. Chernikov [a], W.R. Wampler [b,*], A.P. Zakharov [a], A.E. Gorodetsky [a]

[a] *Institute of Physical Chemistry of the Russian Academy of Sciences, Leninsky pr., 31, 117915 Moscow, Russian Federation*
[b] *MS 1056, Sandia National Laboratories, Albuquerque, NM 87185-1056, USA*

Received 31 March 1998; accepted 12 June 1998

Abstract

Due to their importance for tritium inventories in future DT fueled fusion machines, experimental data on H isotope diffusion, absorption and retention in deep traps ($E_b \cong 4.3$ eV) of graphites exposed to hydrogen at elevated temperatures have been reviewed. Deuterium retention was studied in edge- and basal-oriented pyrolytic graphite (PG) and polycrystalline RG-Ti-91 damaged by irradiation with 200 keV carbon ions. Deuterium loading was done by soaking in D_2 gas at 1473 K, and the resulting D retention was measured by nuclear reaction analysis. The microstructure was studied by cross-sectional TEM, SEM and microprofilometry. The concentration of strong traps created by irradiation and estimated by the amount of accumulated deuterium was shown to saturate with the damage above $\approx$1 dpa at about 1000 appm. In non-damaged and damaged graphites deuterium diffuses via porous grain boundaries and along basal planes within crystallites, while its migration through the graphite lattice along the *c* direction was found to be negligible. Radiation modifications of PG retard deuterium diffusion and decrease the rate of its chemical erosion by a factor of five. The amount of deuterium accumulated in strong traps in graphites is mainly influenced by their macro- and microstructure, while the degree of graphitization seems to be less important. Derivations are made of the susceptibility of damaged graphites, in particular, CFCs to the retention of hydrogen isotopes in deep traps.

1. Introduction

Due to low atomic number and excellent thermal properties carbon [1], carbon-based materials and, in particular, carbon-fiber composites (CFCs) [2] are suitable materials for plasma facing [3] and high heat flux components [4] in fusion reactors. Processes of interaction between hydrogen isotopes (below called 'hydrogen') and graphite are of great concern [5,6]. Among them, hydrogen transport and retention in graphites both before and after neutron irradiation are important for ITER [7] and other future fusion machines.

The microstructure and physical properties of graphites change drastically when damaged at low irradiation temperatures ($T_{irr} \leqslant 573$ K [8]), and differ basically from those of graphites which are undamaged or are damaged at elevated temperatures [1,8–10]. In addition, a wide spectra of traps for hydrogen are created in graphites under irradiation at 300 K [11]. Sorption of hydrogen in damaged and non-damaged graphites from hydrogen gas at high temperatures can give information about hydrogen traps created by irradiation.

The fact that the nature of hydrogen solubility (understood as a measure of accumulated hydrogen) is related to the chemical interaction with C atoms was known long ago [12,13]. Sites which are able to bind hydrogen atoms are available not only in damaged [11], but also in non-damaged graphites [14–16]. On the basis of a strong correlation between hydrogen solubility and the degree of graphitization, Atsumi et al. [17] made the conclusion that the hydrogen adsorption and trapping are related to defects in graphites. Redmond et al. [12] concluded that at elevated temperatures adsorption of H

* Corresponding author. Tel.: +1-505 844 4114; fax: +1-505 844 7775; e-mail: wrwampl@sandia.gov.

0022-3115/99/$ – see front matter
PII: S0022-3115(98)00466-8

atoms occurs on C atoms at the edge of crystallites. Also Hoinkis considered only zig–zag and armchair faces of graphite as a potential area for adsorption [14,15]. Based on his experimental data and a phenomenological approach Hoinkis derived the adsorption enthalpy for deuterium, $\Delta H \cong -2.23$ eV/D_2 which corresponds to the C–D bond energy, $E_b \cong 3.4$ eV.

Hoinkis found that at 1173 K the dependence of the amount of deuterium adsorbed in graphitic Matrix A3-3 on the gas pressure, p_{D_2}, over the range 2.5–2.5 × 10^3 Pa obeys a Langmuir isotherm [14]. A linear relationship between the solubility and $\sqrt{p_{D_2}}$ in a pressure range 1–100 kPa for 1573 K was derived for laminar pyrolytic carbon in Ref. [13]. When investigating deuterium adsorption in Isograph-88 ($T \leqslant 1173$ K) within the pressure range 5–95 kPa Atsumi et al. [18] observed a $\sqrt{p_{D2}}$ dependence of the gas amount contributing to a dominating thermal desorption peak. A similar influence of the hydrogen pressure in a range 5–20 kPa on the hydrogen trapping in neutron irradiated graphite was documented in [19]. On the other hand, Redmond et al. [12] found that the amount of adsorbed gas versus pressure could be approximated by two lines over the pressure range 13.3–1.33 × 10^5 Pa (at $\geqslant 1358$ K) suggesting a very weak dependence at low pressures. Moreover, Causey et al. [16] found that loading of POCO AXF-5Q graphite (POCO) from D_2/T_2 atmosphere at 1473 K gave a retention of 15 appm independent of gas pressure over the range 0.66–66 Pa. A conclusion was made that under the conditions specified the retention of D/T in POCO was determined by the 100% occupation of hydrogen in strong traps which are present in as-manufactured graphite which have a binding energy of 4.3 eV.

Generally, non-monotonic dependence of hydrogen absorption on the loading pressure are attributed to the presence of heterogeneities [12,20]. Kanashenko et al. [21,22] used this idea just to show quantitatively why the amount of hydrogen trapped in graphites during high temperature sorption sometimes does [12–14,18,19], but sometimes does not [16,18] show the dependence on the loading gas pressure. Their model based on the Langmuir type adsorption includes not one, as in Ref. [14], but two trap types: submicroscopic interstitial clusters [8] (strong traps with adsorption enthalpy, $\Delta H = -4.4$ eV/H_2) and usual C atoms at the edge of crystallites ($\Delta H = -2.3$ eV/H_2). The latter value ΔH was estimated taking into account the relaxation of dangling sp^2 bonds. For 1473 K such an approach results in an equilibrium hydrogen retention which is weakly dependent on the hydrogen pressure at pressures $\ll 1$ kPa, shows a much stronger dependence in a range of pressures around 1 kPa and saturates at pressures $\gg 1$ kPa. Two plateaus of the sorption isotherm correspond to complete filling of the two types of adsorption sites characterized by their own concentrations and binding energies. Such an approach removes an apparent contradiction between the above experimental data. The same formalism is applicable to irradiated graphites with appropriate concentrations of the two types of traps [22]. Remaining questions are probably due to uncertainties in sorption kinetics determined by migration characteristics of hydrogen in graphites.

In general, both H_2 molecules and H atoms are able to penetrate and migrate in graphites [6,23–25]. Migration of H atoms in graphite crystals is believed to occur much easier along basal planes than along the c axis even after severe radiation damage [24–27]. Grain boundaries (GBs) can play a role of channels for rapid hydrogen migration [27]. Anisotropic diffusion of hydrogen together with a wide variety of graphite microstructures and a possibility to activate different migration mechanisms are responsible for a great scatter of hydrogen diffusion data in graphites [28]. An attempt to single out the main diffusion channels and to describe the whole variety of experimental data calculating an effective diffusion coefficient was made by Ashida et al. [29]. Radiation damage even after low temperature irradiation up to 10–12 dpa does not eliminate orientation effects [6] of radiation-induced self-diffusion [30], diffusion of tritium atoms [26] and in any case does not lead to a full amorphization [31].

A series of experimental works was focused on the investigation of hydrogen sorption in damaged graphites at relatively high temperatures, that is hydrogen retention in strong traps [17,19,21,22,32–34]. A general scheme of investigations was suggested in Ref. [32]. After production of radiation damage in graphites using neutron or C ion irradiation, the specimens are soaked in a D_2 atmosphere at a temperature of 1473 K [16,28] for a time period which is supposedly enough to attain an equilibrium between the gas and material. If the loading gas pressure is chosen in the range of the first plateau of the sorption isotherm (less than 0.1–1.0 Pa at 1473 K [21,22]) only strong traps become populated. After cooling, the amount of deuterium in specimens is determined by nuclear reaction analysis (NRA) or thermal-desorption spectroscopy (TDS). In most graphites, except HOPG [32,35], some CFCs [17,19,36] and some special pyrolytic graphites [33,34], lattice damage increases the retention of hydrogen isotopes up to 1000–1500 appm. The main conclusions which follow from these and related experiments are given below.

1. Initial microstructure is an important factor for D accumulation at strong traps in damaged graphites [17,19,32–34,36]. Deuterium retention is lower in materials with a higher degree of graphitization [17,19,36].
2. Strong traps are present at typical concentrations of 10–20 appm in all graphites in their original state [16,28,34] and can be created by plastic deformation, fracture [34] and irradiation.

3. Irradiation temperature, having a great bearing upon microstructure [8,9,31], influences the amount of retained deuterium [34].
4. Neutron radiation damage hinders the diffusivity of hydrogen [19,37].
5. At lower temperatures and higher pressures the concentration of accumulated deuterium gets higher [13,19] which is attributed by the authors of [21,22] to the occupation of weaker traps (second plateau at sorption isotherm).
6. Strong traps are considered to be dangling bonds of C atoms [17,19,34] belonging to crystal edges [36] and submicroscopic interstitial clusters [34] formed in the course of radiation damage [8]. This agrees with the presence of sp^3 C–C bonds [33] and sp^3-clusters [10] in damaged graphites.
7. Provided strong traps for hydrogen are identified with those created at RT by neutron irradiation [38] or α particles [31] one can expect their evolution in a temperature range $\geqslant 1773$ K [38] and annealing at 2023 K [31].

The role of initial microstructure in accumulation of deuterium in damaged graphites is less well understood [33]. What is the main reason for a very low sorption of deuterium in BO HOPG [32]: a low concentration of deep traps produced by C ion implantation, or a very slow permeation of deuterium in the direction normal to basal planes which could hinder in part the access of H to deep traps created? What is the nature of the correlation between the degree of graphitisation and the resistance of damaged graphites to hydrogen accumulation [17,19,36]?

In the present work we examine the influence of the graphite microstructure on the accumulation of hydrogen. Experiments similar to those in Refs. [33,34] were done with specimens of EO and BO PG and RG-Ti-91 graphites having the microstructure well documented in [31] and [39], respectively. We demonstrate a leading role of structural factors in both damaged and non-damaged graphites on the accessibility of deep traps by D atoms under loading from D_2 gas at 1473 K, while a degree of graphitization seems to be of minor importance. Graphite damaged by ion irradiation is found to be less permeable for deuterium and more resistant to chemical erosion than non-damaged graphite.

2. Experimental

The pyrolytic graphite (PG) used in this investigation was produced by Le Carbone-Lorraine (France) and had a turbostratic structure and a density of 2.19 g cm^{-3}. Plate-like samples with dimensions of $10 \times 10 \times 1$ mm^3 were cut parallel and perpendicular to the hexagonal c axis, called EO (edge-oriented) and BO (basal-oriented), respectively. Samples of well graphitized anisotropic RG-Ti-91 graphite (below denoted as RGT) produced by NIIGrafit (Russia) were also investigated. The RGT samples were cut parallel and perpendicular to the pressing axis, $\boldsymbol{P}$. Individual grains in RGT are oriented with their c axes predominantly parallel to the $\boldsymbol{P}$ direction [39] and samples cut in different way were also called EO and BO, respectively. After cutting all the samples were mechanically polished using grinding papers and diamond paste and then ultrasonically cleaned in acetone. Ref. [33] gives details of C ion implantation, post-implantation loading with deuterium and subsequent determination of trapped deuterium by nuclear reaction analysis and in Ref. [34] definitions are formulated of deuterium concentrations determined in different parts of a specimen.

Radiation damage was produced at room temperature by 200 keV C ion implantation up to three fluences, $\Phi_1 = 0.37 \times 10^{20}$ ion m^{-2}, $\Phi_2 = 1.83 \times 10^{20}$ ion m^{-2} and $\Phi_3 = 9.13 \times 10^{20}$ ion m^{-2}. According to TRIM [40] calculations the mean projected range of 200 keV C ions in graphite ($\rho = 2.19$ g cm^{-3}) is $R_p \cong 400$ nm, the maximum range, $R^{max} \cong 480$ nm and the straggling, $\sigma \cong 50$ nm. From TRIM calculations the mean damage levels in the ion stopping range are $Kt = 0.25$, 1.30 and 6.45 dpa for the three fluences. The pressure during irradiation was about 5×10^{-4} Pa.

Irradiated graphite samples were exposed at 1473 K to flowing 99.97% pure D_2 gas at a pressure of 0.66 Pa for 1 h. After examination by different methods (see below) all PG samples were exposed to deuterium a second time for 48 h under the same conditions.

Deuterium depth distributions were studied by NRA using the ^{3}He(D,p)α nuclear reaction. A beam of ^{3}He ions ($\cong 1.3 \times 1.3$ mm^2) having energy up to 1.8 MeV was directed onto the sample, and protons from nuclear reactions with D atoms present in the sample were counted. The method of resonance depth profiling [41] is used to determine the distribution of D within 4 μm of the surface from measurements of proton yield versus ^{3}He ion energy. An actual distribution of D atoms in the irradiated part of a specimen was approximated by a step-like three component depth profile characterized by the following parameters: (1) a concentration of D atoms on the irradiated surface (area density), $C_D(S)$ (at/m^2), (2) a uniform concentration of D atoms within the near-surface damaged region from 0 to $R = 0.5$ μm ($\approx R^{max}$) in the depth, $C_D(R)$ (appm), and (3) a uniform concentration of D atoms beyond the damaged region (in the bulk) within a depth range from $R = 0.5$–5 μm, C_D^b (appm). In samples loaded with deuterium at 1473 K, D atoms are found not only in areas irradiated with C ions, but also in areas shielded from C ion beam by clamping springs [34]. The background deuterium distribution in these unirradiated regions was determined assuming the same three component depth profile as for the irradiated regions. The relevant concentration values

were denoted by an additional '0' superscript to the right, and namely: $C_D^0(S)$ – the area density of D atoms on the non-irradiated surface (at/m^2), $C_D^0(R)$ – the uniform concentration of D atoms (appm) in the near-surface layer of 0.5 μm thick and C_D^{0b} – the uniform concentration of D atoms (appm) in the bulk out of the C ion irradiated area. For the sake of rapid comparison of D atom amounts on the surface and in the bulk $C_D^{(0)}(S)$ values are also expressed in concentration units (appm) using the following relation:

$$C_D^{(0)}(S_R) = kC_D^{(0)}(S), \tag{2.1}$$

where $k = 10^6(N_c\ R)^{-1}$ (appm × m^2/at.fract. × at.) is the correlation factor, converting the D atom area density ($C_D^{(0)}(S)$ in units (at m^{-2})) into the ratio of the D atom quantity on the surface to the number of C atoms underlying this surface within a layer of the thickness, $R = 0.5$ μm ($C_D^{(0)}(S_R)$ in units (appm)). Here $N_c = 10^{29}$ m^{-3} is the volume density of C atoms. Let us point out that in Ref. [34] for all graphites studied, the values $C_D(R)$ appeared to be considerably higher than $C_D(S_R)$, and the authors discussed only the values $C_D^{(0)}(R)$. In the present work the values $C_D^{(0)}(S_R)$ for PG appeared to be comparable with $C_D^{(0)}(R)$, and both are discussed below. Besides, the following notation is used: $C_D^{(0)}(S + R) \equiv C_D^{(0)}(S_R) + C_D^{(0)}(R)$.

The microstructure was studied in a Philips EM-430 TEM operated at 300 kV. TEM specimens were obtained using both a planar thinning and cross-section technique. The final stage of specimen preparation was performed by Ar ion milling in a Gatan 600 DuoMill™. The surface morphology was investigated in a Philips SEM-525 equipped by a goniometer-stage and using quantitative analysis of stereo-images produced by secondary electrons. The analysis procedure developed for TEM stereo pair evaluation [42] was corrected for a tilted SED position relative to the electron beam direction. In addition, the surface profile measurements were carried out in a Sloan Technology DekTak^3 ST system.

3. Experimental results

Visual and optical analysis of PG and RGT samples after C ion irradiation and deuterium loading did not change the irradiated surface noticeably if the exposure time was as low as 1 h, while a subsequent exposure of PG specimens for additional 48 h under the same conditions led to significant changes of the surface relief, especially for EO PG samples. Non-irradiated areas of the latter acquired the appearance of black suede, while irradiated areas were more bright. The appearance of BO specimens due to prolonged exposure in D_2 changed to a lesser extent. It was noted that in all the PG specimens after 49 h in D_2 the irradiated surface area protruded over non-irradiated one and they were divided by a step. Polishing traces were distinguishable in areas of EO PG irradiated up to $\Phi = \Phi_{2,3}$, while they were never found in non-irradiated areas. This together with an unusual behavior of $C_D(\Phi)$ dependences for PG specimens loaded for 49 h (Section 3.2) led us to subject these specimens to a detailed analysis in SEM (Section 3.3), by means of precision profilometry (Section 3.4) and by cross-sectional TEM (Section 3.5).

The microstructure of PG and RGT both before and after radiation damage by He ions at RT was studied in detail in Refs. [31] and [39], respectively. In the following section the main features of the virgin microstructure of PG and new experimental results on its evolution due to C ion implantation at 300 K, are presented.

3.1. Microstructure of PG before and after C ion implantation at 300 K

In Fig. 1(a) an optical micrograph of a polished and etched section of EO PG is presented (the etching was done with He ions at 800 K). It is indicative of a stepwise growth mode of PG. The microstructure of PG consists of jet- or drop-like crystalline areas (grains) oriented with their longer axes approximately normally to the substrate. The grains are about 10 μm in diameter. They consist of curved lamellae with mosaic microstructure characterized by a wide scatter of c axes of constituent subgrains around a longer axis of a particular grain. Analysis of selected area diffraction patterns (SADPs) allows us to estimate the angle at the apex of the scatter angle cone, α_c, as about 50–60° (see insert in Fig. 1(b)). Thus, basal planes of BO PG specimens meet the polished surface plane of a section at an average angle, α_s (see also a scheme in Fig. 10). Assuming the grain diameter is 10 μm and the angle α_c is 50–60° one can show easily that $\alpha_s \cong 15$–$20°$. Basal planes of adjacent grains meet each other at angles of 60° forming grain boundaries (GBs). The latter are clearly visualized on TEM micrographs made at low magnifications (Fig. 1(b)). Such a macroarchitecture of PG can lead to situations when in EO PG specimens the matrix at some GBs faces locally the surface with basal planes providing for local preferential etching of GBs during ion thinning of TEM specimens (see also [31]).

Fig. 2 presents TEM micrograph of a cross-sectional specimen prepared from an EO PG sample irradiated with C ions up to $\Phi_2 = 1.83 \times 10^{20}$ ion m^{-2}. The thickness of a layer which has lost its diffraction contrast due to radiation damage, δ_0, is $\geqslant 450$ nm which with an accuracy of 5–6% coincides with R^{max} of 200 keV C ions in PG. In contrast to non-damaged matrix there are no visible cavities within the damaged layer. Besides, according to the analysis of selected area diffraction patterns (cp. SADPs in Fig. 2) the damaged structure is characterized by the mean lattice parameter in c direc-

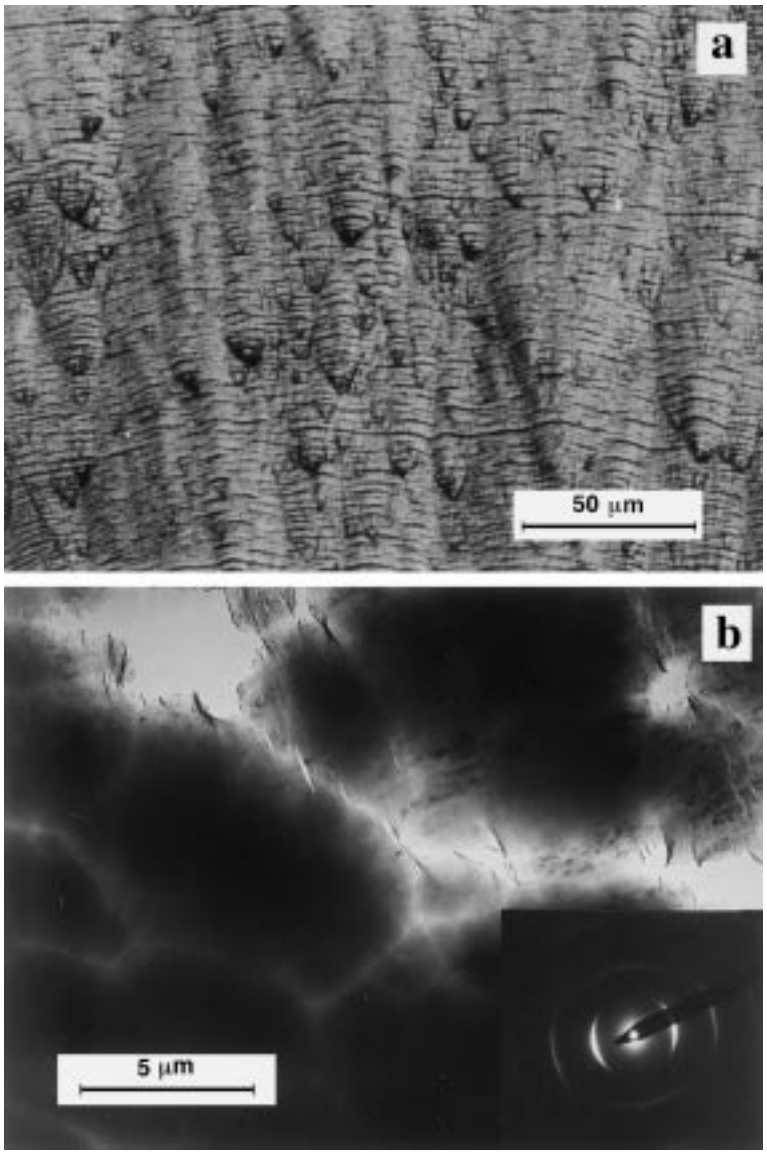

Fig. 1. Macrostructure of EO PG: (a) optical micrograph after etching the surface with He ions at 800 K; (b) TEM micrograph at low magnification (tilt angle, $\varphi = 45°$), in the insert is SADP from an area 6 μm in diameter ($\varphi = 0°$).

tion enlarged to $\geqslant 0.382$ nm as compared to 0.346 nm in the virgin turbostratic PG matrix.

3.2. NRA data

All the data on deuterium concentrations on the surface, $C_D(S)$, in the ion stopping range, $C_D(R)$, beyond this range, C_D^b, and the sum, $C_D(S + R)$, for EO and BO PG samples after C ion irradiation up to three fluences, $\Phi_{1,2,3}$, and soaking into D_2 gas for 1 h and 49 h are presented in Table 1, in four vertical columns, respectively. In the same columns the corresponding values of D concentrations for non-damaged ($\Phi = 0$) areas, $C_D^0(S)$, $C_D^0(R)$, C_D^{0b} and $C_D^0(S + R)$ are given. Table 2 presents concentrations of deuterium retained in EO and BO RGT, in both irradiated and non-irradiated areas, with our earlier data for EO RGT [33] for comparison.

For convenience in comparison between D concentrations at different distances from the surface, x, and at different fluences, Φ, the numerical data of Tables 1 and 2 are partly reflected in diagrams in Figs. 3 and 4, respectively. Fig. 5(a) presents the dependences of the total amount of deuterium retained in the ion stopping range and on the surface, $C_D(S + R)$, versus the fluence,

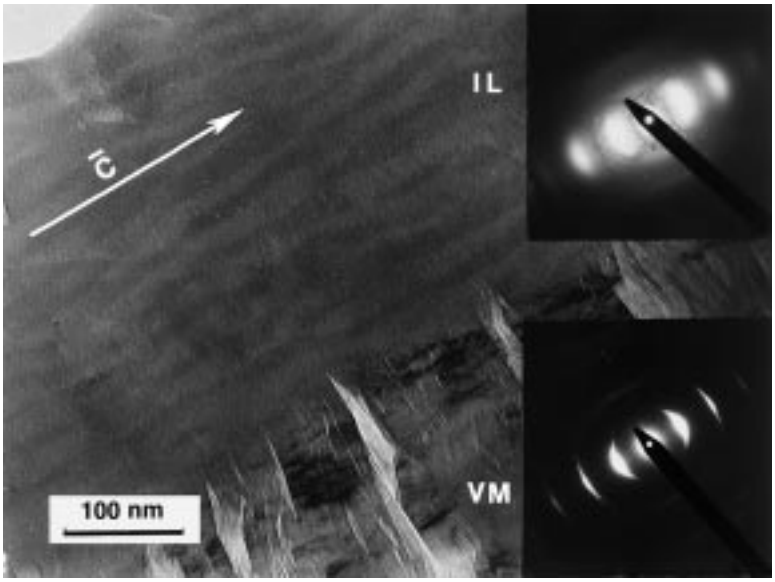

Fig. 2. Cross-sectional view of the microstructure of EO PG sample implanted with 200 keV C ions at 300 K up to a fluence, $\Phi_2 = 1.83 \times 10^{20}$ ion m^{-2}; IL – implanted layer, VM – virgin matrix; SADPs correspond to damaged and non-damaged specimen areas.

Φ, while Fig. 5(b) shows fluence dependences of the amount of deuterium trapped solely within the ion stopping range, $C_D(R)$.

3.2.1. Exposure time, $\tau = 1$ h

For $\Phi_{2,3}$ the values of $C_D(S + R)$ are 2–3 times and the values $C_D(R)$ are 3–4 times higher for EO PG compared to BO PG (Figs. 3 and 5). The values of $C_D(S)$ are approximately the same for both types of PG (cp. $C_D(S_R)$ levels in Fig. 3), showing a tendency to grow with Φ. At $\Phi \leqslant \Phi_2$ they remain below and at $\Phi = \Phi_3$ half as much again as the total area density of adsorption sites on the zig–zag and armchair faces of graphite, $N_S \cong 1.3 \times 10^{19}$ m^{-2} [14] (Table 1). The value of $C_D^0(R)$

Table 1
Mean deuterium concentrations on the surface, $C_D(S)$, in the ion stopping range, $C_D(R)$, beyond this range, C_D^b, and the sum $C_D(S + R)$ in EO and BO PG irradiated with 200 keV C ions up to fluences / mean damage levels indicated and soaked thereafter in D_2 atmosphere ($p_{D_2} = 0.66$ Pa) at 1473 K for exposure times, $\tau = 1$ h and 49 h

	Fluence, Φ (C-ion m^{-2})/ Mean damage level, $K\,t$ (dpa)	$C_D(S)$ ($\times 10^{19}$ D m^{-2})	$C_D(R)$ (appm)	C_D^b (appm)	$C_D(S + R)$ (appm)
EO PG,	$\Phi = 0$ / Non-damaged	0.36 ± 0.05	115 ± 10	6 ± 1	185 ± 20
$\tau = 1$ h	$\Phi_1 = 0.37$ E20 / 0.25	0.73 ± 0.04	140 ± 10	3 ± 1	285 ± 15
	$\Phi_2 = 1.83$ E20 / 1.30	0.66 ± 0.12	760 ± 30	0 ± 2	895 ± 55
	$\Phi_3 = 9.13$ E20 / 6.45	1.80 ± 0.13	600 ± 30	1 ± 2	960 ± 55
$\tau = 49$ h	$\Phi = 0$ / Non-damaged	0.27 ± 0.13	265 ± 30	38 ± 2	320 ± 55
	$\Phi_1 = 0.37$ E20 / 0.25	0.03 ± 0.10	130 ± 20	21 ± 2	135 ± 40
	$\Phi_2 = 1.83$ E20 / 1.30	0.50 ± 0.08	100 ± 20	19 ± 2	200 ± 35
	$\Phi_3 = 9.13$ E20 / 6.45	0.55 ± 0.09	170 ± 20	13 ± 2	280 ± 40
BO PG,	$\Phi = 0$ / Non-damaged	0.27 ± 0.03	10 ± 3	0.4 ± 0.4	64 ± 9
$\tau = 1$ h	$\Phi_1 = 0.37$ E20 / 0.25	0.48 ± 0.05	90 ± 10	0.6 ± 1.0	185 ± 20
	$\Phi_2 = 1.83$ E20 / 1.30	0.69 ± 0.05	165 ± 10	0.0 ± 1.0	305 ± 20
	$\Phi_3 = 9.13$ E20 / 6.45	1.70 ± 0.15	190 ± 35	0.5 ± 0.3	530 ± 65
$\tau = 49$ h	$\Phi = 0$ / Non-damaged	0.07 ± 0.01	18 ± 2	0.2 ± 0.2	32 ± 4
	$\Phi_1 = 0.37$ E20 / 0.25	0.08 ± 0.02	55 ± 5	1.1 ± 0.3	70 ± 10
	$\Phi_2 = 1.83$ E20 / 1.30	0.60 ± 0.06	260 ± 10	0.0 ± 1.0	380 ± 25
	$\Phi_3 = 9.13$ E20 / 6.45	0.71 ± 0.09	330 ± 20	1.9 ± 1.5	470 ± 40

Table 2
Mean deuterium concentrations on the surface, $C_D(S)$, in the ion stopping range, $C_D(R)$, beyond this range, C_D^b, and the sum $C_D(S + R)$ in EO and BO RGT irradiated with 200 keV C ions up to fluences/mean damage levels indicated and soaked thereafter into D_2 atmosphere ($p_{D_2} = 0.66$ Pa) at 1473 K for the exposure time, $\tau = 1$ h with the corresponding data on EO RGT from Ref. [33]

	Fluence, Φ (C-ion m^{-2})/ Mean damage level, $K\,t$ (dpa)	$C_D(S)$ ($\times 10^{19}$ D m^{-2})	$C_D(R)$ (appm)	C_D^b (appm)	$C_D(S + R)$ (appm)
EO RGT, $\tau = 1$ h	$\Phi = 0$ / Non-damaged	0.1 ± 0.1	120 ± 20	9.5 ± 1.5	140 ± 40
	$\Phi_1 = 0.37$ E20 / 0.25	0.0 ± 0.1	400 ± 20	13.0 ± 2.0	400 ± 40
	$\Phi_2 = 1.83$ E20 / 1.30	0.1 ± 0.1	960 ± 20	9.5 ± 1.5	980 ± 40
	$\Phi_3 = 9.13$ E20 / 6.45	0.0 ± 0.1	1040 ± 40	12.0 ± 2.5	1040 ± 60
$\tau = 1$ h [33]	$\Phi = 0$ / Non-damaged	0.05 ± 0.08	165 ± 20	13 ± 1	175 ± 35
	$\Phi_1 = 0.37$ E20 / 0.25	0.0 ± 0.15	430 ± 40	17 ± 6	430 ± 70
	$\Phi_2 = 1.83$ E20 / 1.30	0.40 ± 0.15	1490 ± 40	10 ± 2	1570 ± 70
	$\Phi_3 = 9.13$ E20 / 6.45	0.0 ± 0.20	1470 ± 50	18 ± 3	1470 ± 90
BO RGT, $\tau = 1$ h	$\Phi = 0$ / Non-damaged	0.1 ± 0.05	100 ± 10	7 ± 1	120 ± 20
	$\Phi_1 = 0.37$ E20 / 0.25	0.0 ± 0.2	360 ± 40	13 ± 3	360 ± 80
	$\Phi_2 = 1.83$ E20 / 1.30	0.1 ± 0.1	920 ± 20	9 ± 1	940 ± 40
	$\Phi_3 = 9.13$ E20 / 6.45	0.0 ± 0.2	1180 ± 40	11 ± 4	1180 ± 80

for EO PG is more than one order of magnitude higher than that for BO PG (Fig. 3(a) and (b)). Values of C_D^{0b} and C_D^b for BO PG are below the limit of detection (about 1 appm), while for EO PG the value of C_D^{0b} is slightly above the limit of detection and the values for C_D^b are at the limit of detection.

In contrast to PG, the C_D values are nearly the same for EO versus BO RGT samples, and the surface concentrations of deuterium in both irradiated and non-irradiated areas are negligible (Table 2, Fig. 4). This is in full accord with our earlier data on EO RGT [33] (Table 2). The absolute values $C_D^{(0)}(S + R)$ for RGT are comparable with those for EO PG, but the values $C_D(R)$ at $\Phi_{2,3}$ are half as much again as those for EO PG (Fig. 5(a) and (b)). The values of C_D^{0b} and C_D^b, being somewhat lower than the corresponding values for RGT in Ref. [33], are approximately the same (10–11 appm) for EO and BO RGT. Also, the values C_D^{0b} are about two times higher and C_D^b are much higher than those for EO PG.

3.2.2. Exposure time, $\tau = 49$ h

The extension of exposure time in D_2 gas by 48 h drastically affected all the C_D values of EO PG while those of BO PG changed only moderately (Table 1 and Fig. 5). For instance, for $\Phi = \Phi 2\ \Phi 3$, $C_D(R)$ increased by a factor of about 1.6, whereas $C_D(R)$ for EO PG decreased greatly. At the same time, the values of C_D^{0b} and C_D^b showed a large increase for EO PG but did not change for BO PG, (Table 1).

3.3. SEM data

Fig. 6 shows typical SEM micrographs of EO and BO PG samples (after 49 h exposure at 1473 K in D_2 gas) near the border between irradiated and non-irradiated areas. In all cases non-damaged regions are recessed below damaged regions and a clear etching of both is evident. For EO PG, in agreement with the data of optical microscopy, the roughness of the irradiated surface is much less pronounced compared to that of non-irradiated one (Fig. 6(a)). Due to anisotropy, the surface etching of BO PG specimens proceeds in a different way (Fig. 6(b)), and the difference between surface relief of damaged and non-damaged regions following the gas exposure is not so well-defined as in the case of EO PG.

An attempt was made to measure the heights, Δh, of steps between damaged and non-damaged regions by means of analysis of stereo-pairs taken in SEM. Due to a time consuming procedure this was done only for three specimens: EO PG/Φ_1, EO PG/Φ_2 and BO PG/Φ_3 along directions normal to a border in question. The following results were obtained: Δh_{SM}(EO PG/Φ_1) = 0.60 ± 0.15 μm, Δh_{SM}(EO PG/Φ_2) = 0.75 ± 0.10 μm and Δh_{SM}(BO PG/Φ_3) = 1.0 ± 0.2 μm. To get more comprehensive information on the height of steps at the edge of non-damaged and damaged areas a faster method of microprofilometry was also used.

3.4. Dek Tak data

Examples of the surface microrelief measured for three different PG specimens in directions crossing the edges of C ion beam spots are presented in Fig. 7. The corresponding step heights, Δh_{DT}, are: Δh_{DT} (EO PG/Φ_2) = 0.70 ± 0.05 μm (a), Δh_{DT}(BO PG/Φ_1) = 0.85 ± 0.05 μm (b) and Δh_{DT}(BO PG/Φ_3) = 0.75 ± 0.05 μm (c). For fluences $\Phi_{2,3}$ the values Δh_{DT} for EO and BO PG are approximately the same being with a

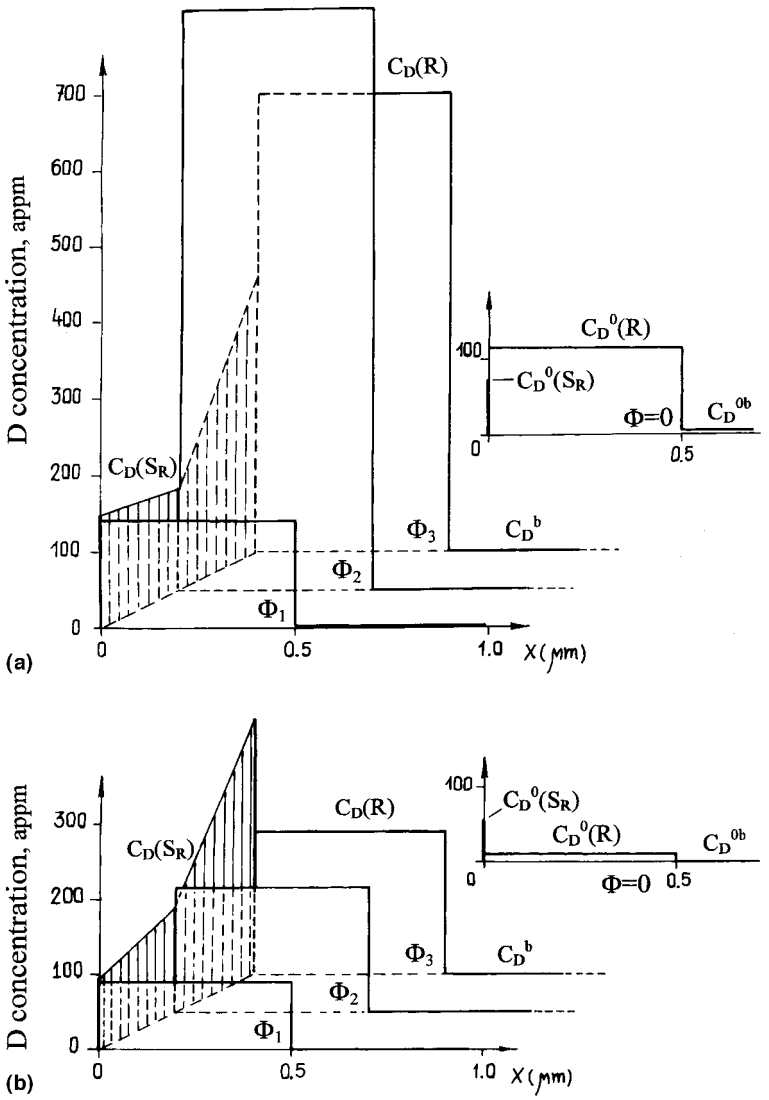

Fig. 3. Diagrams of deuterium depth distributions in EO PG (a) and BO PG (b) in areas non-irradiated and irradiated with 200 keV C ions up to fluences, $\Phi_1 = 0.37 \times 10^{20}$ ion m^{-2}, $\Phi_2 = 1.83 \times 10^{20}$ ion m^{-2} and $\Phi_3 = 9.13 \times 10^{20}$ ion m^{-2} after soaking into D_2 gas at 1473 K and $p_{D_2} = 0.66$ Pa for 1 h.

high degree of confidence between 0.7 and 0.8 μm. The scatter of Δh_{DT} values for $\Phi = \Phi_1$ is higher, but all the available data are within a range from 0.4 to 0.9 μm. Comparison of Δh_{SM} data obtained by means of SEM stereo-pair evaluation with those using Dek Tak system, Δh_{DT}, shows good agreement.

It is evident that the considered steps cannot be caused solely by swelling of the C ion implanted layer. Assuming the radiation induced increase of c lattice parameter, $\Delta c/c \approx 0.1$ (Section 3.1) a maximal protrusion in the case of BO PG cannot exceed $\Delta h_{irr} \approx R^{max} \Delta c/c \approx 50$ nm much smaller than the experimentally measured heights, Δh^{exp}, mentioned above. Thus, one has to attribute the formation of these steps to a carbon chemical erosion (gasification) proceeding noticeably slower in regions modified by the ion irradiation.

3.5. TEM data

The microstructure evolution of radiation modified layers on PG after extended exposure in D_2 gas was investigated in TEM using cross sections. Results are illustrated in Figs. 8 and 9 where micrographs of cross sections of EO PG/Φ_2 and BO PG/Φ_3 specimens, respectively, are presented. The appearance of radiation-modified layers on EO PG imaged in bright (a) and dark

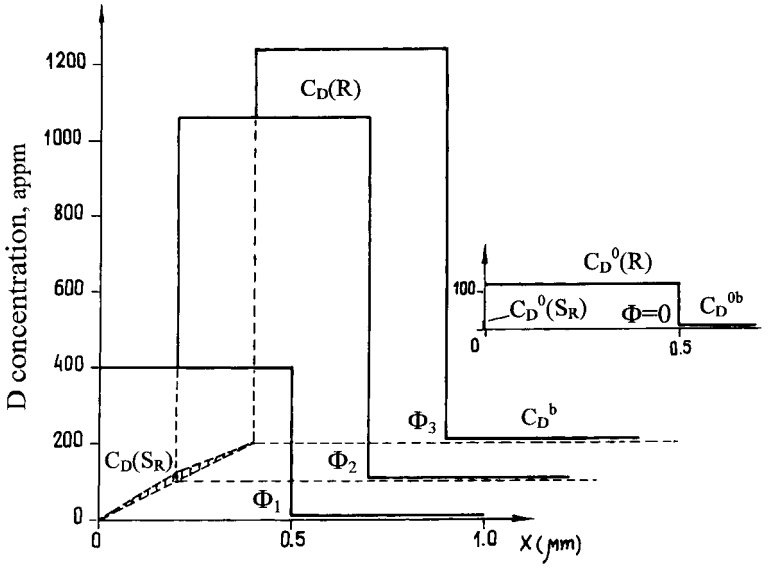

Fig. 4. Diagram of deuterium depth distributions in EO RGT in areas non-irradiated and irradiated with 200 keV C ions up to fluences, $\Phi_1 = 0.37 \times 10^{20}$ ion m^{-2}, $\Phi_2 = 1.83 \times 10^{20}$ ion m^{-2} and $\Phi_3 = 9.13 \times 10^{20}$ ion m^{-2} after subsequent soaking into D_2 gas at 1473 K and $p_{D_2} = 0.66$ Pa for 1 h.

(b) fields (Fig. 8) implies a reduction in their thickness and considerable changes of microstructure after the exposure in D_2 (comparing with Fig. 2). Qualitatively such an appearance is characteristic of all C ion implanted EO PG specimens held in deuterium for 49 h. Based on TEM measurements of several cross sections of EO PG implanted up to $\Phi = \Phi_{2,3}$ the thickness of remaining radiation modified layers, δ, was estimated as 300 ± 50 nm, while for specimens implanted to $\Phi = \Phi_1$ we found $\delta = 200 \pm 50$ nm. In contrast to radiation modified layers of EO PG just after C ion irradiation, the implanted layers after a long D_2 exposure are very friable, especially in their upper part, and contain a very high volume density of thin and extended lenticular and band-like cavities. Some wide orifices reach the underlying non-damaged carbon matrix (Fig. 8, the left-hand side in a,b). The exposure in D_2 gas has practically no influence on the c parameter of damaged carbon.

The microstructure of ion implanted BO PG after exposure in D_2 for 49 h differs considerably from that of EO PG for all fluences (Fig. 9). Radiation modified layers near the surface are not friable, but contain not numerous, separate and, by all appearance, closed lenticular cavities. For all fluences the thicknesses of layers remaining after exposure to D_2 are roughly the same as for EO PG samples. Parameters of empty cavities are reminiscent of those of He filled bubbles in BO PG implanted with 40 keV He ions up to $\Phi = 1.2 \times 10^{21}$ He m^{-2} [31]. In contrast to those in EO PG (Fig. 2), the original lenticular cavities in BO PG could not be completely cured during irradiation because of the lack of compressive stresses in the direction normal to basal planes [31].

Based on the step heights, Δh^{exp} (Δh_{SM} and Δh_{DT}), measured at the edge of ion beam spots and taking into account the thicknesses δ, estimated by TEM, of damaged layers remaining on the surface of ion implanted PG specimens after a long exposure in D_2 one can evaluate more precisely the depth of PG gasification of non-irradiated graphite

$$\Delta h^0 = \Delta h^{exp} + \delta_0 - \delta, \tag{3.1}$$

where δ_0 is taken equal to R^{max}(200 keV C^+). Substituting numerical data one gets readily $\Delta h^0 \approx 1.0 \pm 0.1$ μm. This implies the rate of gasification of non-damaged PG under conditions specified is about 20 nm h^{-1}, while that for damaged PG falls inside the limits 3.5–5.5 nm h^{-1}.

4. Discussion

High concentrations $C_D(R)$ after post-irradiation loading with hydrogen in damaged graphites reported in Ref. [17,19,32–34] and in this work cannot be explained by adsorption on inner surfaces available in virgin graphites. This implies that radiation defects created in the bulk during ion implantation are, even if partly, accessible by H atoms at high temperatures. One of the main effects on graphite by radiation damage at 300 K is the reduction of the crystalline size [39,43,44]. But these newly created intercrystalline sub-boundaries are not

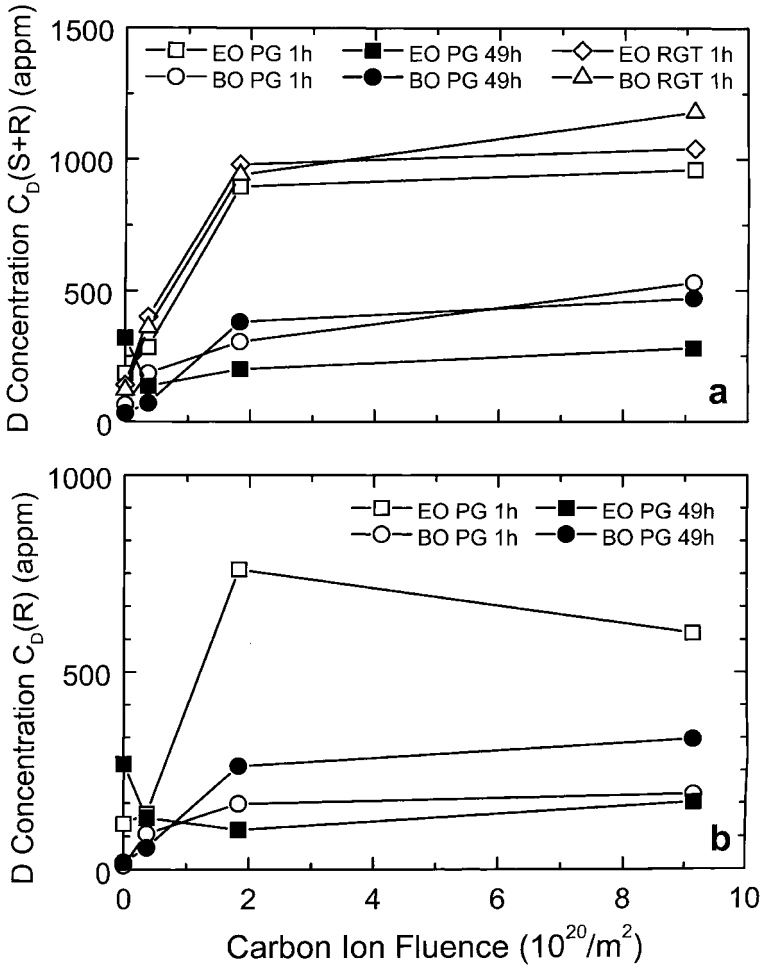

Fig. 5. Deuterium concentrations, $C_D(S + R)$ (a) and $C_D(R)$ (b) in differently oriented PG and RGT specimens versus the fluence, Φ, of C ions. The data of $C_D^0(S + R)$ and $C_D^0(R)$ for $\Phi = 0$ are shown as well.

easy paths for hydrogen diffusion [19,37], probably for the lack of intrinsic free volume. On the other hand, migration of hydrogen along normal (sub)GBs should be considered.

In the following we discuss processes of deuterium retention, migration and chemical erosion in both damaged and non-damaged graphites. Ungraphitized turbostratic PG (deposition temperature is well below graphitization temperature) was used as a highly anisotropic material. Due to original cavities throughout its volume, it has a relatively low value of closed porosity, $\Delta V/V \cong 5 \times 10^{-3}$ [31] with a corresponding specific inner surface area, $S_v \cong 2.4$ m^2 g^{-1} (derived on the basis of cavity parameters in [31] with the use of relation in [45]), and no noticeable free volume is related to its GBs [31]. On the other hand, RGT was chosen which is also an anisotropic, but well graphitized material accumulating a great deal of porosity in GBs [39].

Changes in microstructure of graphites from C ion irradiation (Sections 3.1 and 3.5) are similar to those observed from He ion irradiation at 300 K [31,39]. Atomic displacements induce swelling due to formation of submicroscopic interstitial clusters, and a corresponding c parameter increase. This results in curing of original cavities which is significantly facilitated in EO PG compared to BO PG specimens by strong compressive stresses in the direction of c axis. Submicroscopic clusters are immobile interstitial atom groups containing 2–6 atoms which are not able to grow [8]. According to [34], dangling bonds of C atoms belonging to these clusters are primarily responsible for D atom capturing in deep traps. Indeed, in contrast to dangling bonds at crystal edges or dislocation loops (pointed out as location sites of deep traps in [22,28]), the probability of their mutual relaxation (see e.g. [21]) is minimal. Strengthening of the matrix in c direction is supposed to

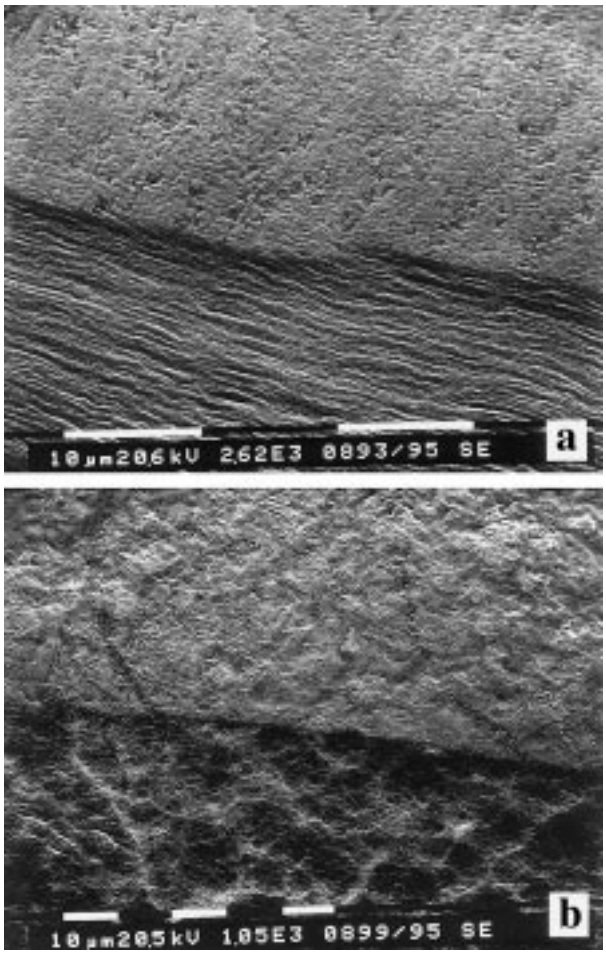

Fig. 6. SEM micrographs (in secondary electrons) of differently oriented PG specimens at the edge of areas irradiated with 200 keV C ions (on top) after exposure at 1473 K in D_2 gas for 49 h: (a) EO PG, $\Phi = \Phi_2$, tilt angle, $\varphi = 25°$; (b) BO PG, $\Phi = \Phi_3$, $\varphi = 20°$. Tilt axis is roughly parallel to the edge of irradiated areas.

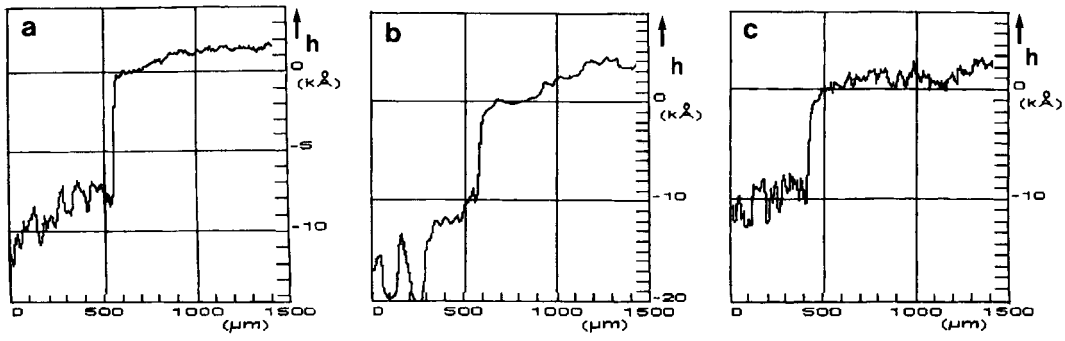

Fig. 7. Surface profiles of PG specimens near the edge of regions irradiated with C ions (to the right hand side) after exposure in D_2 gas at 1473 K for 49 h: (a) EO PG, $\Phi = \Phi_2$, (b) BO PG, $\Phi = \Phi_1$, (c) BO PG, $\Phi = \Phi_3$. Height axes are calibrated in units of $k\mathring{A} = 0.1$ μm.

be a result of interlayer bonding via the same submicroscopic clusters [31,39]. The anisotropy of the PG lattice was shown to remain even after implantation with ions other than C^+ up to more than 10 dpa [31]. In the following discussion, it is assumed as a first approximation, that layers with deuterium concentrations close

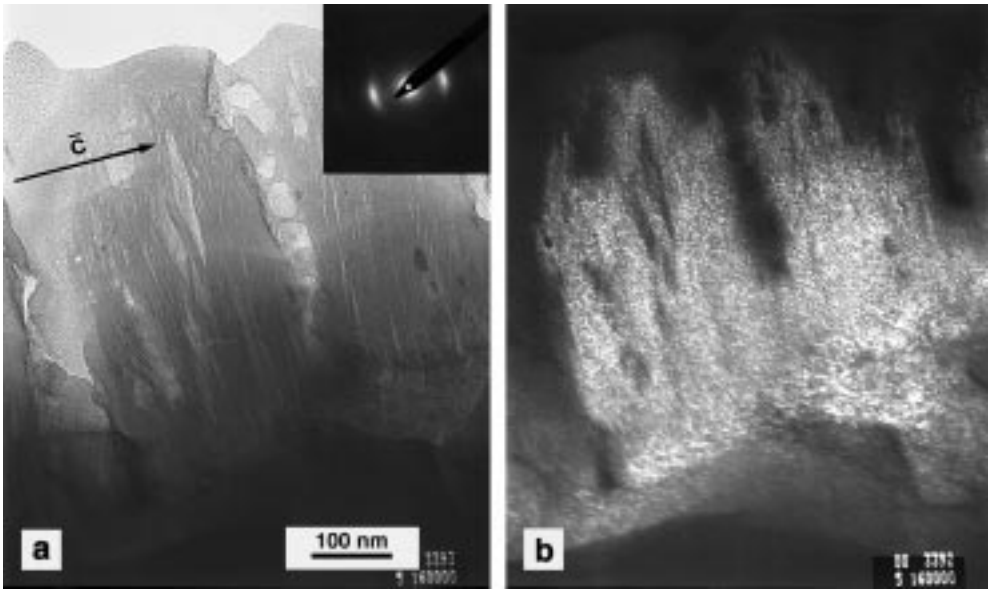

Fig. 8. Cross-sectional view of the microstructure of EO PG sample implanted with 200 keV C ions up to a fluence, $\Phi = \Phi_2$ and exposed to D_2 gas at 1473 K for 49 h: (a) bright field; SADP refers to a selected area of 0.5 μm in diameter and covers partly a virgin matrix; (b) dark field imaged in 002 reflection. Note a very friable microstructure in the upper part of a layer modified by irradiation.

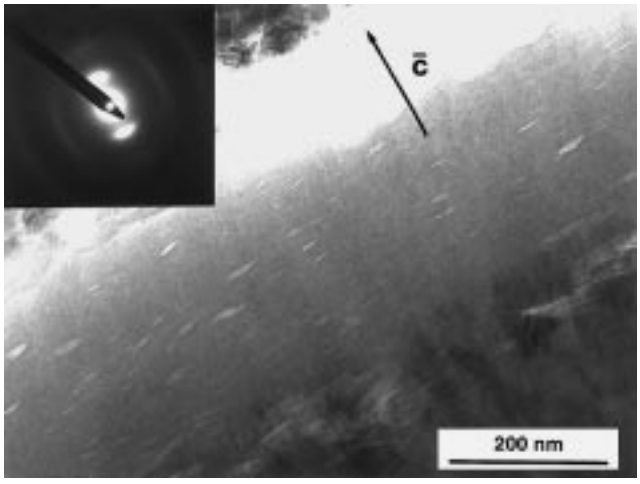

Fig. 9. Cross-sectional view of the microstructure of BO PG sample implanted with 200 keV C ions up to a fluence, $\Phi = \Phi_3$ and exposed to D_2 gas at 1473 K for 49 h. SADP refers to a selected area of 0.5 μm in diameter.

to saturation (100% filling of deep traps) are formed behind a D atom diffusion front which propagates through the graphite matrix.

4.1. Exposure time, $\tau = 1$ h

4.1.1. EO and BO PG

The most striking effect in Section 3.2.1 is a 3–4 fold difference between $C_D(R)$ values for EO and BO PG at $\Phi_{2,3}$ (Fig. 5(b)). Bearing in mind that C ions create in both EO and BO PG approximately the same spatial distribution of defects (in particular, deep traps) and the subsequent soaking in D_2 does not significantly change the microstructure of graphite, the observed difference in $C_D(R)$ is unambiguously attributed to the difference in accessibility of radiation induced deep traps by D atoms migrating from the surface into the bulk of differently oriented PG specimens. Assuming that D atoms diffuse

along but not through basal planes and taking into account that basal planes in BO PG specimens intersect the surface plane at an average angle $\alpha_s \cong 15$–$20°$ (Section 3.1, Fig. 10), one gets readily that the average penetration depth of D atoms into the bulk of BO PG is at least $(\mathrm{Sin}\ \alpha_s)^{-1} \cong 3$–$4$ times less than that for EO PG. This agrees quite well with the experimentally observed difference of corresponding $C_D(R)$ values and implies that the diffusion of deuterium through basal planes proceeds with a much lower diffusion coefficient than along basal planes. Derived from independent experimental results, this deduction agrees well with conclusions on the anisotropy of hydrogen isotope diffusion in a graphite lattice made previously in Refs. [26,27].

If deep traps within the ion range in EO PG implanted to $\Phi_{2,3}$ are assumed to be saturated with deuterium it implies that the mean depth of D atom advance and trapping in deep traps in BO PG is not in excess of $x = R \times \mathrm{Sin}(\alpha_s) \cong 140$ nm.

In the situation where the traps are strong and are filled by propagation of a D atom diffusion front into the matrix, the thickness of the saturated layer behind the front is

$$x = [D_{\mathrm{eff}} t]^{1/2}, \tag{4.1}$$

where

$$D_{\mathrm{eff}} = 2D_m C_m / C_t, \tag{4.2}$$

D_m is the diffusivity of the mobile or untrapped D, C_m is the concentration of mobile D at the surface determined in our case by equilibrium with the gas i.e. the solubility, and C_t is the concentration of traps. The effective diffusion coefficient, D_{eff} , of deuterium in BO PG at 1473 K can thus be estimated to be $D_{\mathrm{eff}}^{\mathrm{BO}} \cong 5 \times 10^{-18}$ m^2 s^{-1} which is two orders of magnitude less than D_{eff}(1473 K) for laminar carbon in Ref. [13]. The fact that this value is two orders of magnitude smaller than the value reported in Ref. [13] may be due to a larger trap concentration from the C ion irradiation in our material, since D_{eff} is inversely proportional to the trap concentration (Eq. (4.2)). An additional reason for such a difference in diffusion coefficients might be a lower density and more porous microstructure of laminar carbon ($\rho = 1.89$ g/cm^3) used in [31] compared to the PG ($\rho = 2.19$ g/cm^3) used here.

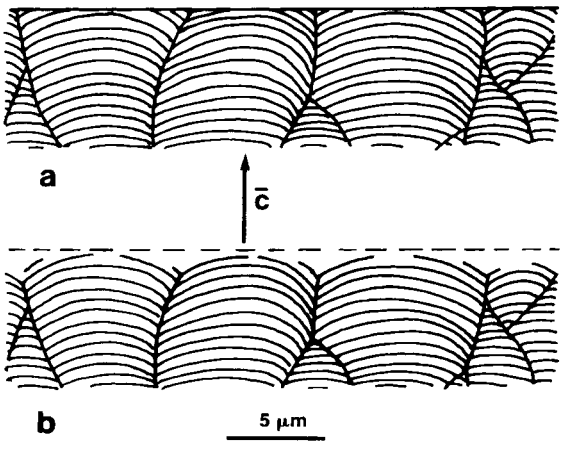

Fig. 10. Schematic presentation of a mechanically polished BO PG sample in cross section before (a) and after (b) chemical erosion in D_2 gas for 49 h. Curved lines denote as-grown piles of basal planes (cp. with Fig. 1(a)). Dashed line in (b) denotes an original position of the surface.

Comparison of deuterium concentrations retained in non-damaged areas of EO and BO PG specimens (cp. $C_D^0(R)$ in Fig. 3(a) and (b)) does not contradict the above conclusion that D atom migration depends strongly on crystallographic orientation. A higher value $C_D^0(R)$ for EO PG is caused, first, by a greater penetration depth of D atoms and also by more lattice deformation, compared to BO PG, created near the surface during specimen polishing [31] (see Section 1).

A decrease of $C_D(R)$ in EO PG by about 20% when increasing Φ from Φ_2 to Φ_3 can be a consequence of growing disorder within the C ion implanted layer which makes the implanted layer less permeable for D atoms. In BO PG such an effect is not observed because within the estimated range of D atom penetration (~140 nm) the mean damage level is about four times lower than that around $R_p = 400$ nm [40]. Besides, if high compressive stresses due to lattice damage play a role in the suppression of D diffusivity in EO PG, such a factor is practically absent in BO specimens [31].

Whereas the values of C_D^{0b} and C_D^b for BO PG are negligible, the corresponding values for EO PG are non-zero (Table 1). In contrast to $C_D^0(R)$, their comparison gives more correct and convincing arguments in favor of the orientation dependence of deuterium diffusion into graphite lattice. Based on the fact that C_D^{0b} in EO PG is 6 ± 1 appm to a depth of at least 4 μm, a rough estimation of a minimum effective diffusion coefficient of D atoms along basal planes yields $D_{\mathrm{eff}}^{\mathrm{EO}} \approx 5 \times 10^{-15}$ m^2 s^{-1}. The difference between C_D^{0b} and C_D^b for EO PG is an indication that radiation damage in the near-surface layers retards transport of deuterium through them. This is in agreement with a conclusion made in Refs. [37,19]. In addition to the influence of traps on D diffusion discussed above, curing of original cavities which short-circuit the near-surface layers in original EO PG and, build up of compressive stresses, may also influence D transport in graphite. The same effects occur for a longer exposure time as well (see Section 4.2.2).

The values C_D(S) for specimens irradiated up to fluences $\Phi_{1,2,3}$ and for non-irradiated specimens are practically the same for EO and BO PG (Fig. 3(a) and (b)). It means that the activity of the outer surface to hydrogen adsorption on differently oriented specimens is

practically the same. $C_D(S)$ values that are relatively high, show a tendency to increase with Φ and at Φ_3 are even higher than the maximal area density of adsorption sites on smooth surfaces of EO PG, $N_S \cong 1.3 \times 10^{19}$ m^{-2}. This surface D might not all be bound in strong traps (non-relaxed dangling C bonds), since trap sites on the surface are still accessible to D at lower temperatures where D could be retained by weaker traps, associated with *relaxed* C bonds (with $E_b < 4.3$ eV), during cooling (see Section 1). Data of the present study and unpublished results of [33] allow us to conclude that after D_2 exposure at high temperatures deuterium concentration on the surface of well graphitized materials (RGT, PO-CO) is noticeably smaller than on the surface of non-graphitized ones (PG, USB-15, PGI). The origin of this difference is not yet clear.

4.1.2. EO and BO RGT

Experimental data on all the C_D values including those in non-damaged areas are practically the same for EO and BO RGT, respectively (Table 2, Fig. 5). This is stipulated by porous GBs which play a role of channels for rapid migration of deuterium into the bulk followed by a slower interplanar diffusion of D atoms into interior of individual (sub)grains and, in this way, obliterates all the differences between differently oriented RGT specimens. Against this background, the role of crystallite boundaries as deuterium conductors in PG seems to be negligible, which is reasonable taking into account different microstructure of GBs in PG and RGT (see introduction to Section 4).

Absolute values of $C_D(R)$ and C_D^b for RGT are noticeably higher than those for EO PG. This seems to be natural taking into account the above role of GBs in RGT. Another possible reason for this observation is a less efficient hindering of D atom migration within a damaged RGT due to a stress relaxation at the expense of a great deal of porosity present in its GBs [39] (Section 4.1.1). The equality of C_D^{0b} and C_D^b in RGT is another argument for the absence of retardation of deuterium migration through the ion stopping range.

4.2. Exposure time, $\tau = 49$ h

4.2.1. Carbon chemical erosion (gasification)

From the lower values of $C_D(R)$ for BO PG compared to EO PG after 1 h gas exposure we inferred that D did not diffuse all the way through the damaged zone in BO PG due to kinetically limited transport. To test this hypothesis, the EO and BO PG samples were exposed to D_2 gas for an additional 48 h (1473 K, $p_{D_2} = 0.66$ Pa). For kinetically limited D uptake the longer loading time should result in deeper permeation of D into the material and hence higher values of $C_D(R)$ in the irradiated BO PG. NRA analysis showed that for $\Phi = \Phi 2\ \Phi 3$, $C_D(R)$ increased by a factor of about 1.6, whereas $C_D(R)$ for EO PG decreased greatly. A change in the visual appearance of specimens after prolonged exposure in D_2 led us to closely examine their surface microstructure (Sections 3.3–3.5, Figs. 6–9). It was found that removal of material from the surface by gasification of carbon took place with rates of 20 nm h^{-1} for non-damaged carbon and about 4 nm h^{-1} for damaged carbon. The five fold difference in removal rates implies that radiation modification of graphite gives rise to a noticeable increase of resistance towards gasification.

In general, at high temperatures and hydrogen pressures of 1 Pa, graphite reacts with hydrogen yielding under equilibrium acetylene and methane, but in negligible quantities [14]. On the other hand, we used for gas loading not a constant D_2 volume, but a constant gas flow which continuously displaced the equilibrium between deuterocarbons and deuterium providing for a constant rate of deuterocarbon formation and surface chemical erosion. Besides, we used deuterium with a purity 99.97% without any further purification, and some erosion due to carbon oxidation and hydrogenation could be a reason for an additional erosion of graphite [46]. Anyway, it does not change the conclusion concerning the effect of radiation modification of graphite on its resistance towards gasification. It seems to have similar roots with the effect of radiation-induced strengthening of PG in the *c* direction [31,39] and, hence, with the presence of submicroscopic interstitial clusters [8].

Due to gasification the thickness of radiation modified layers is reduced for 49 h D_2 exposure by 200–300 nm, approximately equally for EO and BO specimens (Section 3.5). However, microstructural changes differ considerably between differently oriented specimens which shows that the crystalline anisotropy still persists after irradiation (see Section 1).

4.2.2. EO PG

Radiation modified layers on EO PG specimens exposed to D_2 for 49 h are extremely friable (Fig. 8). We failed to make rigorous determination of the open porosity in such layers, but tentatively, based on rough estimates, this value in upper parts of the layers reaches $\geqslant 50\%$. So, the experimentally measured values $C_D(R)$ for EO PG (Fig. 5(b)) reflect mean deuterium concentrations in radiation modified layers which are very friable and thinner compared to those after 1 h exposure. To get true values of deuterium concentration within the remaining portion of the damaged layer after erosion, a correction factor, k', has to be introduced for the discrepancy between the thickness of the NRA analysis range, R, and a thickness of deuterium rich layer, δ', corrected for its porosity ($\delta' < \delta$), and namely: $k' \cong R/\delta'$. Such estimates based on experimental values $C_D(R)|_{\Phi 2,3}$ roughly correlate with deuterium concentrations at sat-

uration, that is with $C_D(R)|_{\Phi 2,3}$ values for EO PG exposed in D_2 for 1 h. In other words, a concentration of deep traps created by ion irradiation does not decrease noticeably in the matrix of radiation modified graphite during annealing at 1473 K for 48 h which is in accord with *a high thermal stability of deep traps* (see Section 1).

The value $C_D^0(R)$ as a measure of deep trap concentration near the surface of non-damaged EO specimen (Table 1) seems to be anomalously high. This effect is related to a surface relief which develops more intense and deeply (up to a depth of $>R$) during gasification in non-damaged regions compared to that in damaged regions. The latter follows from TEM observations and is noticeable in SEM (cp. upper and lower parts in Fig. 6(a)). Thus, after gasification the near-surface layers of non-irradiated EO carbon present a very large surface area for adsorption of D atoms. The same would apply to weaker traps at the surface which might be filled during cool-down.

$C_D^0(R)$ was shown to be unsuitable for identification with the background deep trap concentration in PG. For characterization of the latter the only reliable values are C_D^{0b} and C_D^b. While the value $C_D^{0b} \cong 38$ appm (Table 1) is still influenced by the surface relief due to gasification, the values C_D^b for $\Phi_{2,3}$ with the mean value $C_D^b \cong 16$ appm seem to be representative for the background deep trap concentration, that is in the bulk of as-received PG. This value is comparable with C_D^b values for RGT and POCO determined in [34].

With the minimum effective diffusivity of D along basal planes of $D_{eff}^{EO}(1473\ K) \cong 5 \times 10^{-15}\ m^2\ s^{-1}$ (Section 4.1.1), D should be present in EO specimens to depths of at least 30 μm after exposure to D_2 for 49 h.

4.2.3. BO PG

A cross-sectional view of a C ion implanted BO PG sample is shown in Fig. 9. Fig. 10 presents schematically the microstructure of a mechanically polished BO PG specimen in cross section before (a) and after (b) gasification. This scheme for a non-damaged area is also applicable for a damaged region (with a lesser thickness of gasified layer). The construction of this schema is based on the results of optical microscopy (Section 3.1, Fig. 1(a)) and analysis of BO PG specimens after D_2 exposure in SEM (Section 3.3, Fig. 6(b)). Gasification of a mechanically polished surface proceeds by attacking edge C atoms and further chemical etching of newly created BO surfaces. The selectivity in attacking edge C atoms holds for both hydrogenation and oxidation [46]. The process converts a uniformly polished plane surface (Fig. 10(a)) into a curved and etched one (Fig. 10(b)) having one peculiarity: most of the surface area faces the environment with basal planes stretching to a great degree continuously. Etching craters up to some tenths of a micron deep are permanently available on curved (sub)grain surfaces and provide for their further gasification. In the following discussion, experimental data on C_D in BO PG are explained assuming that deuterium permeability in the c direction is negligible (see Section 4.1.1).

The values $C_D(R)$ for $\Phi = \Phi_{2,3}$ relating to the exposure time, $\tau = 49$ h are a factor of 1.7 higher than those for $\tau = 1$ h (Table 1, Fig. 5(b)). This seems to be a combined result of losses of previously trapped deuterium through gasification and further accumulation of D atoms at strong traps in the remaining damaged layer by migration along basal planes. Taking into account a correction procedure in Section 4.2.2 the above values $C_D(R)$ were shown to indicate that for additional 48 h the mean thickness of a deuterium containing layer (within the remaining portion of the damaged layer on BO PG) has increased from $x \cong 140$ nm at $\tau = 1$ h (Section 4.1.1) to $x \geqslant 240$ nm. In the BO specimen implanted to $\Phi = \Phi_1$ a competition between deuterium accumulation and removal led after $\tau = 49$ h to a reduced amount of retained gas compared to that after $\tau = 1$ h, presumably due to a higher gasification rate of a less damaged matrix (Section 4.2.1).

In spite of the fact that the background concentration of deep traps in PG is 16 appm (Section 4.2.2) the values C_D^{0b} and C_D^b remained in all BO specimens after the exposure for 49 h at a level of detection limit of NRA method (Table 1). This is a strong evidence in favor of both an extremely low sorption through basally oriented perfect surface areas and negligible permeability of basal planes in PG for D atoms at 1473 K.

The value $C_D^0(S + R)$ for 49 h is two times less than that for $\tau = 1$ h which indicates that the number of near-surface traps in unirradiated BO PG has decreased due to gasification of material damaged by mechanical deformation during sample preparation. The non-zero C_D^0 value suggests that the surface of BO specimens subjected to a long exposure in D_2 is not free of such defects as chemically etched craters (Fig. 10(b)). These craters provide for not only rapid gasification of carbon, but also for its saturation up to a certain depth with deuterium.

4.3. General remarks on hydrogen sorption at elevated temperatures

Some authors ignore significant intercrystalline sorption and solution of deuterium in graphites [12,14] and, hence, give little attention to processes of intercrystalline diffusion of D atoms. The results of the present work relating to PG argue directly in favor of these effects. Indeed, if the main paths of deuterium inward migration were (sub)GBs, interconnected pores, channels etc., one could expect in EO PG the lower or, at least, the same permeability and retention of D atoms as in BO PG, due to high compressive stresses and full curing of original pores in the former [31]. In fact, the

opposite is the case, which points out, first, a negligible role of any inner surfaces or closed porosity for deuterium transport in PG. Secondly, the differences in the sorption kinetics of deuterium in EO and BO PG specimens must result from the different lattice orientation of individual (sub)grains relative to the sorption surface in them. In other words, we have to assume transgranular diffusion (followed by trapping in defects) of D atoms in PG, which proceeds much easier in directions along basal planes than normal to them. This effect seems to be of general importance (see also [26,27,30]), but is most commonly obscured by a short-circuiting role of porous GBs in polycrystalline graphites, as occurs for example in RGT, where no differences in sorption kinetics have been observed between EO and BO specimens.

It is believed that crystallite boundaries in HOPG, as well as in carbon fibers (for CFC manufacturing [47]), are even more perfect than those in PG and, hence, are even more resistant towards hydrogen penetration. Then, one can understand the origin of very low deuterium concentrations measured in deep traps of BO HOPG [32] taking into account, in addition to a strong anisotropy of D migration, a high perfection of BO surfaces produced by cleavage of HOPG and a relatively short time of soaking into D_2 gas (3 h). Low tritium concentrations in BO HOPG were found also in [35], in spite of a contribution to the total gas retention of weak traps [22,35].

At long exposure times in hydrogen the gasification of graphites seems to proceed in a steady state mode. In this case the rates of gasification – of 20 and 4.5 nm h^{-1} for non-damaged and damaged PG, respectively, may appear somewhat lower for BO PG and higher for EO PG due to different area densities of edge C atoms (Fig. 10(b)) [46]. Nevertheless, based on the assumption of a negligible permeability of basal planes for D atoms and taking into account that GBs in PG are poor deuterium conductors, the penetration of deuterium into the bulk of EO PG is expected to be much more efficient compared to BO PG. Moreover, in BO PG the depth to which deuterium will be able to advance is expected to be limited by the height of surface discontinuities (craters of chemical erosion).

Many CFCs consist of carbon fiber bundles (tens of vol.%) and highly graphitized carbon matrix formed by carbon deposition onto the bundle preform [47,45]. Such a carbon matrix and the individual fibers (except at the ends) are confined and, hence, face surroundings and adjacent inner pores with basal planes [49,50]. This, combined with anisotropic sorption of D, may be the reason for low retention of deuterium observed in many CFCs and for the very low tritium sorption in neutron irradiated CFCs FMI 222 and MKC-1 PH in Ref. [36] rather than considerations of a high degree of their graphitization offered by the authors. Besides, generally, carbon fiber refer to non-graphitizable materials [48].

On the other hand, an effective transport of hydrogen along carbon fibers, accompanied by its accumulation in deep traps, will occur in fibers facing a gas or plasma volume with their ends. So, 1D-CFCs with a volume fraction of fiber bundles up to ≈80% and a highest thermal conductivity along bundle axis [49] (comparable to that of EO PG along basal planes) are expected to be very vulnerable in respect to hydrogen accumulation. Experimental data in Ref. [28] on high temperature tritium retention in CFC BF Goodrich 2D Weave subjected to plasma irradiation ($E = 100$ eV, $\Phi = 2 \times 10^{24}$ ion m^{-2}, $p_{gas} = 0.66$ Pa, sample orientation was not quoted) do not differ too much from those in POCO. According to our view, in general, hydrogen accumulation in CFCs depends primarily on their macro- and microstructure and the way of hydrogen loading, particularly the orientation of the fibers at the exposed surfaces.

The amount of deuterium accumulated in the ion range of RGT for 1 h is higher than that for EO PG and the more so for BO PG at all fluences (cp. $C_D(R)$ in Figs. 3 and 4). The same holds also if surface deuterium is taken into account and $C_D(S + R)$ values are considered (Fig. 5(a)). A commonly held point of view, that more highly graphitized materials retain less D [17,36], predicts behavior opposite to our observations that PG, a non-graphitized material retains less D than RGT which is highly graphitized ($c \cong 0.330$ nm [39]). Moreover, previous studies show that D retention is lower in other non-graphitized pyrolytic graphites, namely USB-15 (B doped) before [50] and after irradiation [33] and irradiated PGI [33], than in RGT and POCO which are more highly graphitized. Our work provides direct evidence of highly anisotropic deuterium diffusion in the graphite lattice and the important role of GBs for deuterium penetration into the bulk. The hindered transport of deuterium in the c direction together with the spherulite microstructure of USB-15 and PGI and the nature of boundaries between crystalline areas therein [51,33], can account for the low deuterium retention in these materials. The presence of boron in USB-15 may also contribute to its extremely low deuterium retention [33]. These results seriously call into question the widely accepted general assumption that the degree of graphitization is the principle factor determining hydrogen retention in graphites.

5. Summary of results and conclusions

NRA was used to examine the retention of deuterium in EO and BO PG ($\rho = 2.19$ g cm^{-3}) and polycrystalline highly textured EO and BO RGT specimens after irradiation with 200 keV C ions up to mean damage levels 0.25, 1.30 and 6.45 dpa. Deuterium loading was done by exposure to D_2 gas at 1473 K and a pressure 0.66 Pa for

1 h and 49 h. The surface relief and the microstructure of near-surface layers were studied in SEM, by microprofilometry and cross-sectional TEM. In this way the accessibility of deep traps by D atoms in the course of deuterium sorption was examined.

After exposure to D_2 gas D atoms are trapped in the bulk of EO PG significantly deeper than in BO samples which holds for both non-irradiated and irradiated specimen areas. Whereas in EO PG D atoms are present at distances of 4 μm from the surface already after 1 h exposure ($C_D^b \cong 6$ appm), they cannot be found in BO PG at distances ≈0.5 μm even after exposure in D_2 for 49 h. At the same time, the accumulation of deuterium in polycrystalline RGT was independent of specimen orientation. The concentration of deep traps in the ion range saturates at a level of 1000 appm in agreement with the literature data [32–34].

The above and some other experimental results point out that under conditions specified D atoms are mobile along basal planes, while the latter are practically impermeable for D atoms in the *c* direction. This is in accord with a conclusion made by Saeki [26]. Intercrystalline boundaries in PG are very poor conductors of D atoms, while porous (sub)grain boundaries in RGT are channels for rapid deuterium (also in the form of D_2 molecules) migration from which D atoms penetrate suitably oriented adjacent grains and migrate into their bulk along basal planes.

Direct evidence is found on retardation of deuterium diffusion in a graphite matrix damaged by irradiation which agrees with conclusions made in Refs. [19,37]. Chemical erosion (gasification) of PG is noticeable after exposure in flowing D_2 gas (99.97% purity) for 49 h. Radiation modification of graphite provides for approximately five fold decrease of its gasification rate compared to a non-damaged carbon. The anisotropy of both damaged and non-damaged PG manifests itself by the appearance due to chemical erosion of surface relief which differs remarkably for EO and BO specimens. The near-surface layers in EO PG are distinguished from those in BO PG by a heavy friability and deeply developed open porosity.

In the course of deuterium loading from D_2 gas, carbon gasification does not prevent the diffusion of D atoms deep into the bulk of EO PG specimens with the diffusion coefficient, $D^{EO}(1473\ K) \geqslant 5 \times 10^{-15}$ m^2/s, which is close, for the chosen temperature, to the best fit value in [28] (2×10^{-14} m^2/s. Under the same conditions D atoms may be presumed to penetrate BO PG specimens, but not further than up to a depth equal to the mean height of craters of chemical etching (of tenths of a micron). So, one expects a limited accumulation of deuterium (including capturing at deep traps) in the bulk of BO PG specimens subjected to a long exposure in D_2 gas. Tentatively, a limited retention of deuterium in deep traps is also expected for materials in which crystallites or crystalline areas face the environment with basal planes and are tightly bound one with another. Some types of carbon fibers for reinforcement of CFCs, CFC matrix produced by carbon vapor deposition (CVD) and pyrolytic graphites consisting of tangential microspherulites (e.g. USB-15) are examples of such materials.

The background deuterium concentration occupying deep traps in as-received PG was found to be ≈16 appm which is comparable with the values in well graphitized RGT. A relation between the amount of retained gas and a degree of graphitization was noticed only for deuterium chemisorbed on the outer surface and bound there presumably in non-deep (relaxed) traps. Analysis of experimental data of the present and other works relating to deuterium retention in well graphitized and non-graphitized carbon materials implies the following. Deuterium retention in the bulk of both non-damaged and damaged graphites is mainly determined by their macro- and microstructure (mean grain size, porosity, the state of intercrystalline boundaries, texture etc.) and deuterium loading conditions, but only to minor extent by a degree of their graphitization.

Acknowledgements

Specimen preparation and TEM investigations were fulfilled in IFF/KFA, Jülich (Germany) in the group of Professor H. Ullmaier whose attention and support of this work are kindly acknowledged. The authors are grateful to Mr M. Gebauer and Mr W. Michelsen (ISI/KFA) for carrying out the implantations with C^+ ions, Mrs E.M. Würtz for making micrographs in SEM and Mr H.J. Bierfeld for microprofilometry measurements. The authors thank Dr A.V. Markin (IPhCh RAS) for reading the manuscript and making useful comments. Sandia is a multiprogram laboratory operated by Sandia Corporation, a Lockheed Martin Company for the United States Department of Energy under contract DE-AC04-94AL85000.

References

[1] B.T. Kelly, Physics of Graphite, Applied Science, London, 1981.
[2] Essentials of Carbon-Carbon Composites, in: C.R. Thomas (Ed.), Royal Society of Chemistry, Cambridge, 1993.
[3] R. Matera, G. Federici and the ITER Joint Central Team, Design Requirements for Plasma Facing Materials in ITER, in: Fusion Reactor Materials. Abstracts of ICFRM-7, Obninsk, RF, SSC of RF, IPP, Obninsk, 25–29 September 1995, p. 8.
[4] P.G. Valentine, R.E. Nygren, R.W. Burns, P. Rocket, A.P. Colleraine, R.J. Lederich, J. Bredley, High Heat Flux Testing of CFC Composites for the Tokamak Physics Experiment, ibid, p. 75.

[5] K.L. Wilson, W.L. Hsu, J. Nucl. Mater. 145–147 (1987) 121.
[6] W. Möller, J. Nucl. Mater. 162–164 (1989) 138.
[7] T.J. Dolan, ITER. In-vessel tritium source with graphite and tungsten plasma facing components, EDF, No.:ITER/US/95/TE/SA-5 29 March 1995.
[8] B.T. Kelly, J. Vac. Sci. Technol. A4 (3) (1986) 1171.
[9] V.V. Goncharov, N.S. Burdakov, Yu.S. Virgiljev, V.I. Karpukhin, P.A. Platonov, Irradiation Impact on Nuclear Reactor Graphite, Atomizdat, Moscow, 1978, in Russian.
[10] T. Tanabe, Physica Scripta T64 (1996) 7.
[11] B.L. Doyle, W.R. Wampler, D.K. Brice, J. Nucl. Mater. 103/104 (1981) 513.
[12] J.P. Redmond, P.L. Walker, Jr., J. Phys. Chem. 64 (1960) 1093.
[13] R. Causey, T.S. Elleman, K. Verghese, Carbon 17 (1979) 323.
[14] E. Hoinkis, J. Nucl. Mater. 182 (1991) 93.
[15] E. Hoinkis, J. Nucl. Mater. 183 (1991) 9.
[16] R.A. Causey, M.I. Baskes, K.L. Wilson, J. Vac. Sci. Technol. A 4 (3) (1986) 1189.
[17] H. Atsumi, M. Iseki, T. Shikama, J. Fac. Sci. Technol. Kinki Univ. 28 (1992) 221.
[18] H. Atsumi, Sh. Tokura, M. Miyake, J. Nucl. Mater. 155–157 (1988) 241.
[19] H. Atsumi, M. Iseki, T. Shikama, J. Nucl. Mater. 191–194 (1992) 368.
[20] B.M.W. Trapnell, Chemisorption, Butterworth, London, 1955.
[21] S.L. Kanashenko, A.E. Gorodetsky, V.N. Chernikov, A.V. Markin, A.P. Zakharov, B.L. Doyle, W.R. Wampler, in: Proceedings of the Seventh ICFRM, Obninsk, 25–29 September 1995, J. Nucl. Mater. 233–237 (1996) 1207.
[22] S.L. Kanashenko, A.E. Gorodetsky, A.P. Zakharov, Phys. Scripta T64 (1996) 36.
[23] G. Federici, C.H. Wu, J. Nucl. Mater. 186 (1992) 131.
[24] S. Chiu, A.A. Haasz, J. Nucl. Mater. 196–198 (1992) 972.
[25] A.A. Haasz, P. Franzen, J.W. Davis, S. Chiu, C.S. Pitcher, J. Appl. Phys. 77 (1) (1995) 66.
[26] M. Saeki, J. Nucl. Mater. 131 (1985) 32.
[27] K.N. Kushita, I. Youle, A.A. Haasz, J.A. Sawicki, J. Nucl. Mater. 179–181 (1991) 235.
[28] R.A. Causey, J. Nucl. Mater. 162–164 (1989) 151.
[29] K. Ashida, K. Watanabe, J. Nucl. Mater. 183 (1991) 89.
[30] B. Söder, J. Roth, W. Möller, Phys. Rev. B 37 (1988) 815.
[31] V.N. Chernikov, W. Kesternich, H. Ullmaier, J. Nucl. Mater. 227 (1996) 157.
[32] W.R. Wampler, B.L. Doyle, R.A. Causey, K.L. Wilson, J. Nucl. Mater. 176/177 (1990) 983.
[33] V.N. Chernikov, A.E. Gorodetsky, S.L. Kanashenko, A.P. Zakharov, W.R. Wampler, B.L. Doyle, J. Nucl. Mater. 217 (1994) 250.
[34] V.N. Chernikov, A.E. Gorodetsky, S.L. Kanashenko, A.P. Zakharov, W.R. Wampler, B.L. Doyle, J. Nucl. Mater. 220–222 (1995) 912.
[35] H. Kwast, H. Werle, C.H. Wu, Phys. Scripta T64 (1996) 41.
[36] R.A. Causey, W. Harbin, D. Taylor, L. Sneed, Phys. Scripta T64 (1996) 32.
[37] M. Saeki, Int. J. Appl. Radiat. Isot. 34 (1983) 739.
[38] J.H.W. Simmons, Radiation Damage in Graphite, Pergamon, Oxford, 1965, p. 64.
[39] V.N. Chernikov, A.P. Zakharov, H. Ullmaier, J. Linke, J. Nucl. Mater. 209 (1994) 148.
[40] J.P. Biersack, L.G. Haggmark, Nucl. Instr. and Meth. 174 (1980) 257.
[41] S.M. Myers, G.R. Caskey, D.E. Rawl, R.D. Sisson, Metall. Trans. A 14A (1983) 2261.
[42] V.N. Chernikov, PhD thesis, Institute of Physical Chemistry of the Academy of Sciences of the USSR, Moscow, 1980, in Russian.
[43] Y. Gotoh, H. Shimizu, H. Murakami, J. Nucl. Mater. 162–164 (1989) 851–855.
[44] T. Tanabe, S. Muto, Y. Gotoh, K. Niwase, J. Nucl. Mater. 175 (1990) 258.
[45] V.N. Chernikov, W. Kesternich, H. Ullmaier, Macrostructure and microstructure of the carbon fibre composite UAM92-5D-B, J. Nucl. Mater. 244 (1997) 1.
[46] J.M. Thomas, Investigation of carbon oxidation by microscopy, in: Chemistry and Physics of Carbon, P.L. Walker Jr. (Ed.), Marcel Dekker, New York, 1965.
[47] Essentials of Carbon–Carbon Composites, C.R. Thomas (Ed.), Royal Society of Chemistry, Cambridge, 1993.
[48] J.-B. Donnet, R.Ch. Bansal, Carbon Fibres, 2nd ed., Marcel Dekker, New York, 1990.
[49] D.A. Bowers, J.W. Sapp, J. Nucl. Mater. 191–194 (1992) 305.
[50] R.A. Causey, W.R. Wampler, O.I. Buzhinskij, J. Nucl. Mater. 196–198 (1992) 977.
[51] V.N. Chernikov, V.Kh. Alimov, A.E. Gorodetsky, V.M. Sharapov, A.P. Zakharov, E.I. Kurolenkin, J. Nucl. Mater. 191–194 (1992) 320.